

Supporting Information for

**Spontaneous Open-circuit Voltage Gain of Fully Fabricated Organic Solar Cells Caused by Elimination of Interfacial Energy Disorder**

Rui Sun,<sup>a,#</sup> Dan Deng,<sup>b,#</sup> Jing Guo,<sup>a</sup> Qiang Wu,<sup>a</sup> Jie Guo,<sup>a</sup> Muming Shi,<sup>a</sup> Kui Shi,<sup>c</sup> Tao Wang,<sup>d</sup>  
Longjian Xue,<sup>c</sup> Zhixiang Wei,<sup>b\*</sup> Jie Min<sup>a\*</sup>

R. Sun, J. Guo, Q. Wu, J. Guo, M. Shi, Prof. J. Min

<sup>a</sup>The Institute for Advanced Studies, Wuhan University, Wuhan 430072, China

E-mail: [min.jie@whu.edu.cn](mailto:min.jie@whu.edu.cn)

Dr. D. Deng, Prof. Z. X. Wei

<sup>b</sup>CAS Key Laboratory of Nanosystem and Hierarchical Fabrication, CAS Center for Excellence in Nanoscience, National Center for Nanoscience and Technology, Beijing 100190, China

E-mail: [weizx@nanoctr.cn](mailto:weizx@nanoctr.cn)

Dr. Kui Shi, Prof. L. J. Xue

<sup>c</sup>The Institute of Technological Science and School of Power and Mechanical Engineering, Wuhan University, South Donghu Road 8, Wuhan 430072, China

Prof. T. Wang

<sup>d</sup>School of Materials Science and Engineering, Wuhan University of Technology, Wuhan 430070, China

## Experimental Section

**Materials:** BTID-2F<sup>[1]</sup> was provided by Zhixiang Wei' group. Donor materials, including H11,<sup>[2]</sup> J71,<sup>[3]</sup> J52-2F,<sup>[4]</sup> Si-PCPDTBT,<sup>[5]</sup> P3HT,<sup>[6]</sup> PDTSTPD,<sup>[7]</sup> PBDB-T,<sup>[8]</sup> PTB7,<sup>[9]</sup> PTB7-Th,<sup>[10]</sup> P3TDPP,<sup>[11]</sup> PCDTBT,<sup>[12]</sup> and PCE11,<sup>[13]</sup> and acceptor materials, including PCBM, PC<sub>71</sub>BM, IDIC and ITIC, were purchased from Solarmer Materials Inc. Zinc acetate dehydrates, 2-methoxyethanol, and ethanolamine was provided by Sigma Aldrich. ZnO nanoparticle ink was purchased from Nanograde Ltd. Solvents (chloroform and methanol) were dried and distilled from appropriate drying agents prior to use.

**Fabrications of OSCs:** The inverted devices were fabricated with a structure of ITO/ZnO/Active layer (1.3:1, wt%) /MoOx/Ag. Patterned ITO substrates were cleaned with methylbenzene, deionized water, acetone and isopropyl alcohol in an ultrasonic bath for 10 min each. The ZnO precursor solution was prepared by dissolving 0.14 g of zinc acetate dihydrate ( $\text{Zn}(\text{CH}_3\text{COO})_2 \cdot 2\text{H}_2\text{O}$ ) and 0.5 g of ethanolamine ( $\text{NH}_2\text{CH}_2\text{CH}_2\text{OH}$ ) in 5 ml of 2-methoxyethanol ( $\text{CH}_3\text{OCH}_2\text{-CH}_2\text{OH}$ ). A thin layer of ZnO precursor was spin-coated at 5,000 rpm. onto the ITO surface. After being baked at 200 °C for 30 min, the substrates were transferred into a nitrogen-filled glove box. The thickness of ZnO is about 30 nm. For the BTID-2F:PC<sub>71</sub>BM system, the mixture of BTID-2F and PC<sub>71</sub>BM with total concentration ca. 18 mg/ml (donor:acceptor=1.3:1) stirred at 60 °C in chloroform for ca. 0.5 h until they are intensively dissolved. Chloroform was dried and distilled from appropriate drying agents prior to use. The processes of the purification of chloroform are as followed: The purifications involve washing with water for several times to remove the ethanol, drying with potassium carbonate, refluxing with calcium chloride, and then distilling. The distilled CF was stored in the dark to avoid photochemical formation of phosgene. Subsequently, the active layer was spin-coated from chloroform solutions of blends. The thicknesses of active layer is about 90nm. The solar cells were completed by thermal evaporation of ca. 10 nm MoOx and then 100 nm Ag at 10<sup>-6</sup> mbar. The active layer of devices is 4 mm<sup>2</sup>. For the other BHJ OSCs, the detailed processing conditions of their photoactive layers deposited on the surface of the ZnO layer can be found in relevant cited references.

Conventional devices were fabricated with a structure of glass/ITO/PEDOT:PSS/Active layer (1.3:1, wt%) /Ca/Al. The ITO-coated glass substrates were cleaned by the same procedure with inverted devices. A thin layer of PEDOT:PSS was spin-coated at 4,000 rpm onto the ITO surface. After being baked at 150 °C for 15 min under ambient air, the substrates were transferred into a nitrogen-filled glove box. The thickness of PEDOT:PSS is about 40 nm. The mixture of BTID-2F and PC<sub>71</sub>BM with total concentration ca. 18 mg/ml (donor:acceptor=1.3:1) stirred at 60 °C in chloroform for ca. 0.5 h until they intensively dissolved. Subsequently, the active layer was spin-coated from blend chloroform solutions of BTID-2F and PC<sub>71</sub>BM. Finally, a layer of ~20 nm Ca and then 100 nm Al layer was evaporated under high vacuum (10<sup>-6</sup> mbar). The active area of devices is 4 mm<sup>2</sup>.

**Device Characterization:** The current-voltage measurements were performed via the solar simulator (SS-F5-3A, Enlitech) along with AM 1.5G spectra, which was calibrated by the certified standard silicon solar cell (SRC-2020, Enlitech) at 100 mW/cm<sup>2</sup>. The light source was calibrated by using a silicon reference cell. All cells were tested in a nitrogen atmosphere. The thickness of the films was measured with a profilometer (Tencor Alpha Step D 100).

**Material and Film Characterizations:** Atomic Force Microscopy (AFM) images were obtained by using Nano Wizard 4 atomic force microscopy (JPK Inc. Germany) in Qi mode to observe the surface morphologies of the different store timed blend films deposited on glass substrates. Absorption spectra of the different store time blend solid thin films were measured on a Perkin Elmer Lambda 365 UV-Vis spectrophotometer. Photoluminescence (PL) data were collected using a Zolix Flex One Spectrometer. The PL excitation wavelength was set to 405 nm. XPS data were obtained using a Thermo Fisher Scientific ESCALAB250Xi (Thermo Fisher Scientific, UK) using a monochromated Al Ka source. All spectra were recorded using a charge neutralizer to limit differential charging. The main carbon peak is charge referenced to 284.5 eV. The 2-D GIWAXS data were obtained on a XEUSS SAXS/ WAXS SYSTEM (XENOCS, France) at the National Center for Nanoscience and Technology (NCNST, China).

**Impedance spectra Characterizations:** Impedance measurements were measured using the ModuLab XM electrochemical workstation (AMETEK, UK) under a series of voltages with the amplitude of 10 mV from 1 MHz to 100 Hz under one AM 1.5 G illumination conditions.

**SCLC Measurements:** Electron and Hole mobilities were measured using the space charge limited current (SCLC) method, the ITO substrates were ultrasonicated in the same way for solar cell and the architecture: Glass/ITO/ZnO/BTID-2F:PC<sub>71</sub>BM/Ca/Al for electron mobility (Glass/ITO/PEDOT: PSS/BTID-2F: PC<sub>71</sub>BM/MoO<sub>x</sub>/Ag for hole mobilities) measurement was prepared. The mobilities were obtained by taking current–voltage curves and fitting the results to a space charge limited form. The reported mobility data are average values over the five cells at a given film composition.

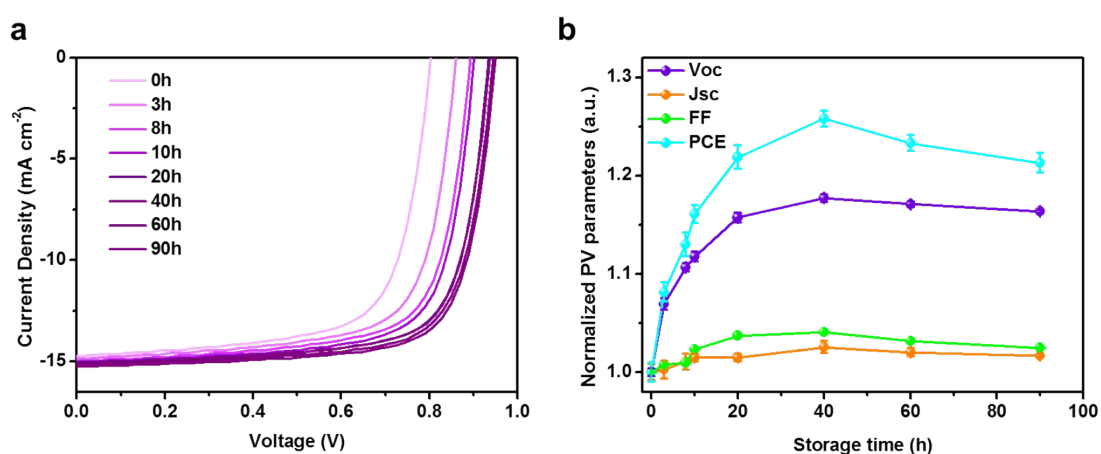
**Photo-CELIV measurements:** In photo-CELIV measurements, the devices were illuminated with a 405 nm laser diode. Current transients were recorded across the internal 50 Ω resistor of our oscilloscope. Here, a fast electrical switch was used to isolate the device, in order to prevent carrier extraction or sweep out. After the variable delay time, the switch connected the device to a function generator. It applied a linear extraction ramp, which was 60 μs long and 2.0 V high. Moreover, it started with an offset matching the  $V_{oc}$  of the device for each delay time.

**TPV and CE measurements:** A 405 nm laser diode was used to keep the devices in approximately  $V_{oc}$  conditions. Driving the laser intensity with a waveform generator (Agilent 33500B) and measuring the light intensity with a highly linear photodiode allowed reproducible adjustments of the light intensity with an error below 0.5% over a range from 0.15 to 2.5 suns. A small perturbation was induced with a second 405 nm laser diode driven by a function generator from Agilent. The intensity of the short (60 ns) laser pulse was adjusted to keep the voltage perturbation below 10 mV, typically at 5 mV. After the pulse, the voltage decays back to its steady state value in single exponential decay. The characteristic decay time was determined from a linear fit to a logarithmic plot of the voltage transient, and returned the small perturbation charge carrier lifetime. In CE measurements, a 405 nm laser diode illuminated the device for 200 μs, which was sufficient to reach a constant  $V_{oc}$  with steady state conditions. At the end of the illumination period, an analogue switch was triggered that switched the solar cell from open-circuit to short-circuit (50 U) conditions within less than 50 ns.

**TPC measurements:** BTID-2F:PC<sub>71</sub>BM solar cells were excited with a 405 nm laser diode. The transient photocurrent response of the devices at short circuit condition to a 200 μs square pulse from the LED with no background illumination. The current traces were recorded on an

ektronix DPO3034 digital oscilloscope by measuring the voltage drop over a 5 ohm sensor resistor in series with the solar cell. DC voltage was applied to the solar cell with an MRF544 bipolar junction transistor in common collector amplifier configuration.

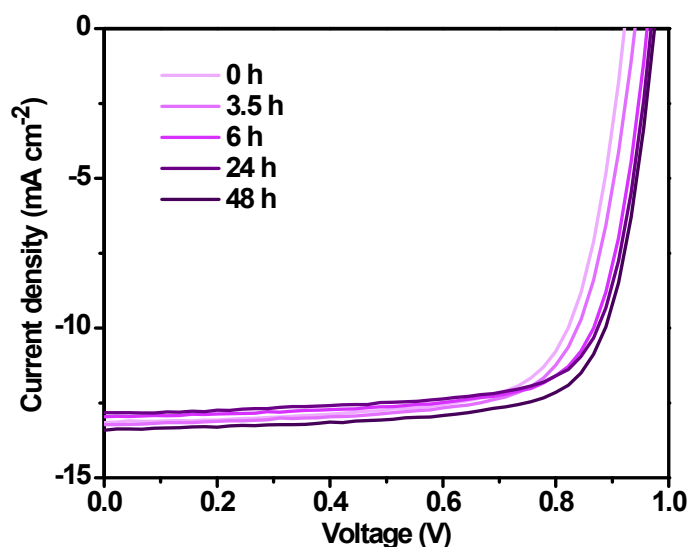
**Contact angle measurements:** Contact angle measurements were performed using water or ethylene glycol contact angle measurement system (Attension Theta Lite), and the surface energy was calculated using the equation of state.



**Supplementary Figure 1.** (a) The time evolution of  $J$ - $V$  characteristics of optimized BTID-2F:PC<sub>71</sub>BM OSCs illuminated under simulated AM1.5G illumination in different time periods; (b) The normalized values of photovoltaic parameters of relevant solar cells as mentioned in (a).

**Supplementary Table 1.** Summary of device parameters of ITO/ZnO/BTID-2F:PC<sub>71</sub>BM/MoOx/Ag solar cells measured under one sun illumination within different time periods.

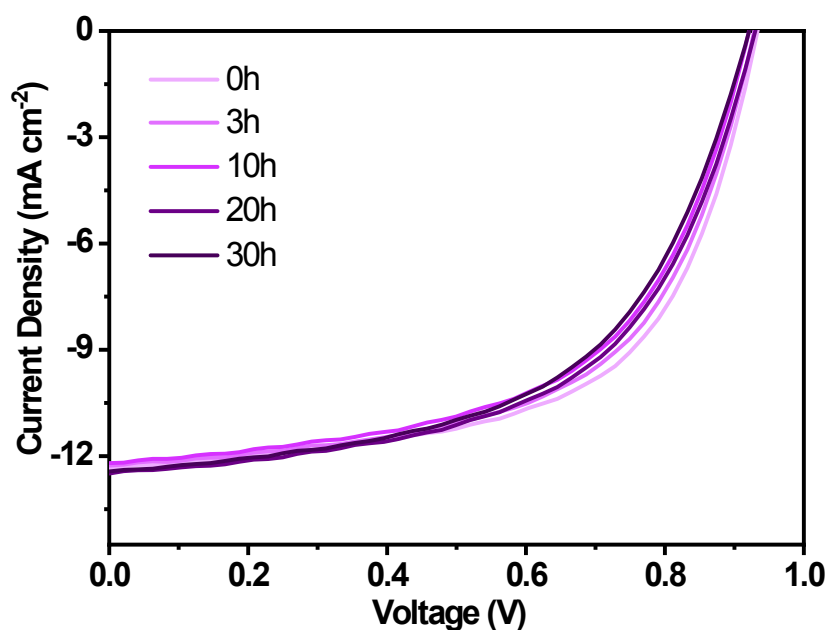
Device test time	$V_{oc}$ [V]	$J_{sc}$ [mA/cm <sup>2</sup> ]	FF [%]	PCE(average) [%]
0	0.807	14.81	70.68	8.45(8.23)
3h	0.863	14.85	71.23	9.14(9.04)
8h	0.893	14.97	71.35	9.55(9.40)
10h	0.902	15.03	72.33	9.81(9.78)
20h	0.934	15.03	73.31	10.30(10.18)
40h	0.950	15.19	73.57	10.63(10.52)
60h	0.945	15.11	72.92	10.42(10.38)
90h	0.939	15.06	72.43	10.25(10.22)



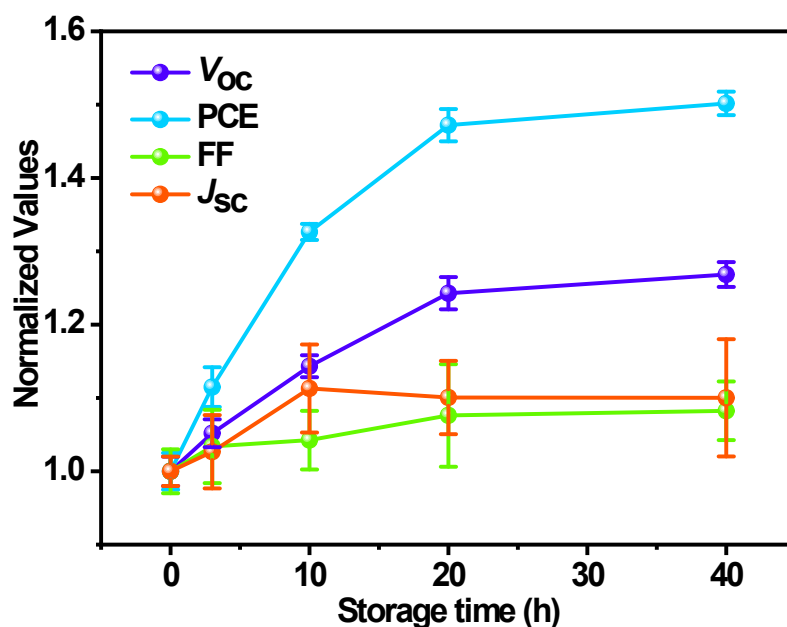
**Supplementary Figure 2.** The time evolution of  $J$ - $V$  characteristics of inverted BDIT-2F:PC<sub>71</sub>BM OSCs illuminated under simulated AM1.5G illumination in nitrogen. The samples were measured in Wei's lab.

**Supplementary Table 2.** Summary of device parameters of ITO/ZnO/BDIT-2F:PC<sub>71</sub>BM/MoO<sub>x</sub>/Ag devices with different time periods measured under one sun illumination.

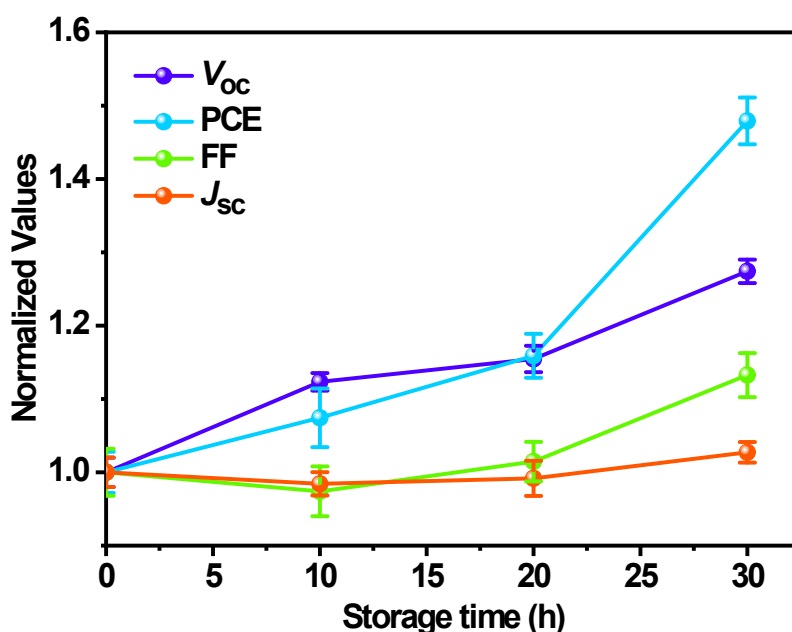
Device test time	$V_{oc}$ [V]	$J_{sc}$ [mA/cm <sup>2</sup> ]	FF [%]	PCE [%]
0	0.897	13.12	72.93	8.58
3.5h	0.916	13.22	72.87	8.82
6h	0.937	12.97	72.89	8.86
24h	0.944	12.84	73.45	8.90
48h	0.950	13.41	73.23	9.33



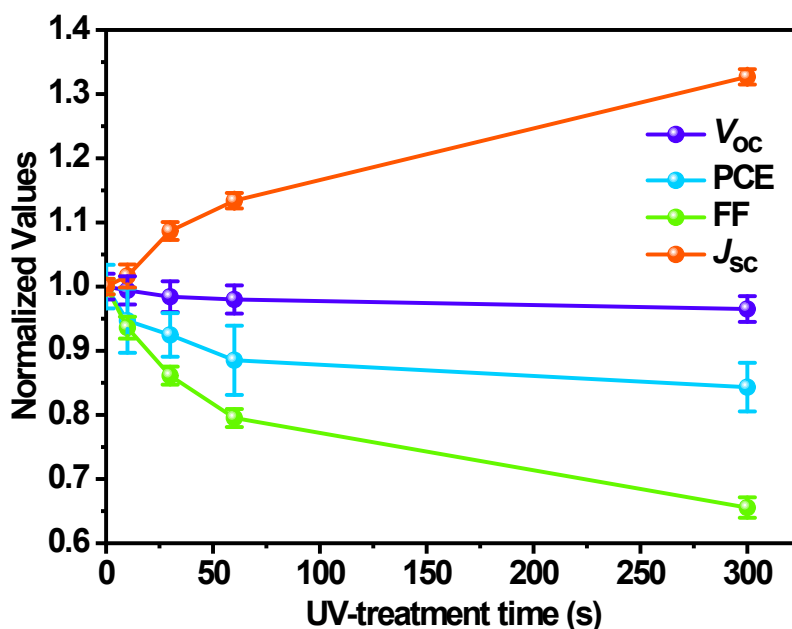
**Supplementary Figure 3.** The time evolution of  $J$ - $V$  characteristics of conventional BTID-2F:PC<sub>71</sub>BM OSCs measured under simulated AM1.5G illumination in different time periods. These samples were also stored in the dark and in nitrogen glovebox.



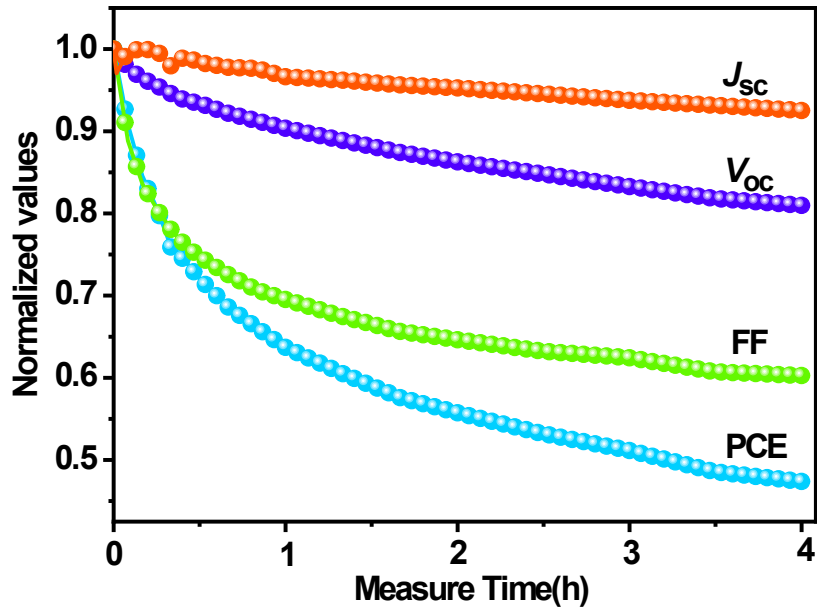
**Supplementary Figure 4.** The normalized values of photovoltaic parameters of ITO/ZnO/BTID-2F:PC<sub>71</sub>BM/Ag OSCs over time measured under one sun illumination within different time periods. These samples were also stored in the dark and in nitrogen glovebox.



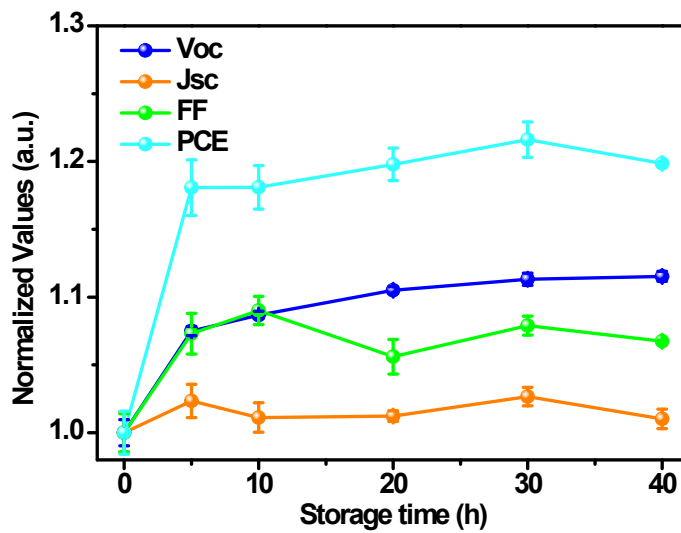
**Supplementary Figure 5.** The normalized values of photovoltaic parameters of ITO/ZnO/BTID-2F:PC<sub>71</sub>BM/MoO<sub>3</sub>/Ag fresh OSCs measured under one sun illumination. Relevant active layers coated on the top of ZnO substrates were stored in different time periods before the MoO<sub>3</sub>/Ag anode depositions.



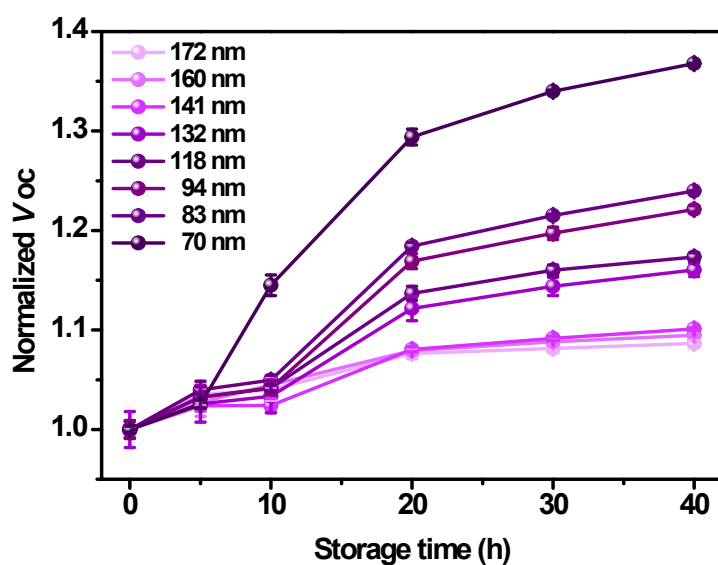
**Supplementary Figure 6.** The normalized values of photovoltaic parameters of ITO/ZnO/BTID-2F:PC<sub>71</sub>BM/MoO<sub>3</sub>/Ag fresh OSCs treated under UV-light within different time periods, and then measured under one sun illumination.



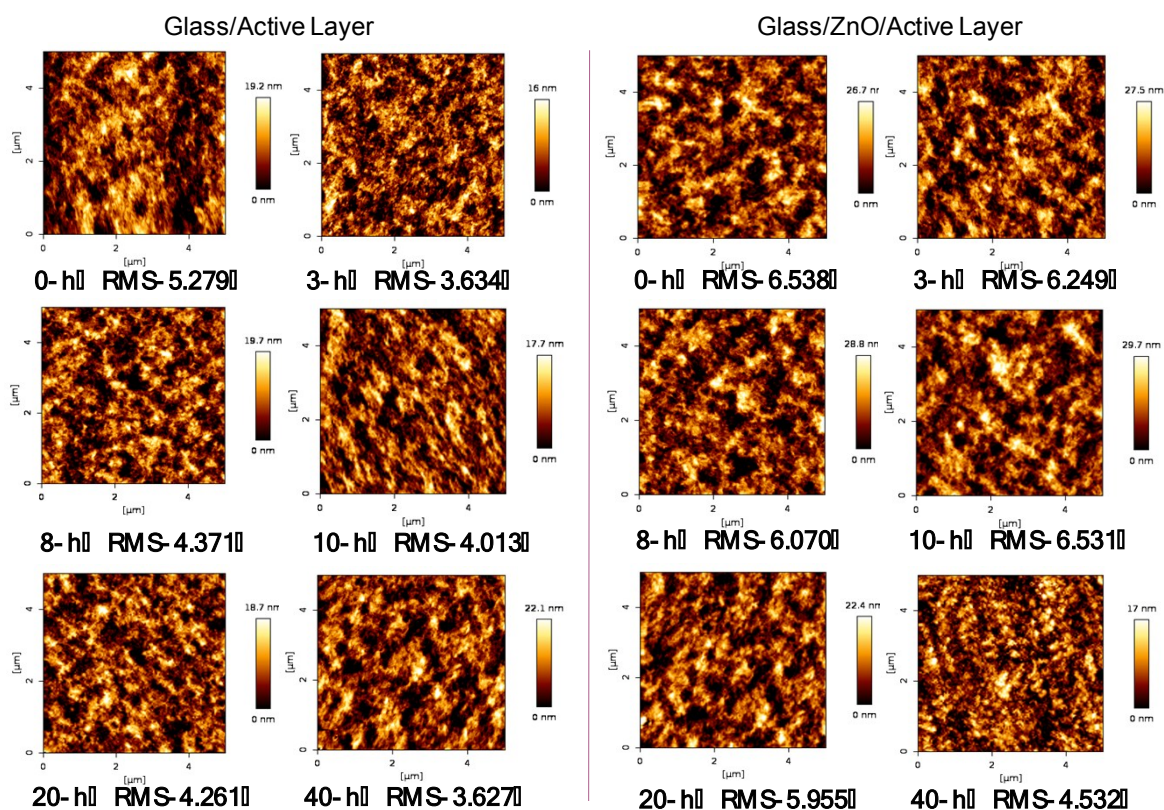
**Supplementary Figure 7.** The normalized values of photovoltaic parameters of ITO/ZnO/BTID-2F:PC<sub>71</sub>BM/MoO<sub>3</sub>/Ag OSCs measured under sustained one sun illumination within 4 h.



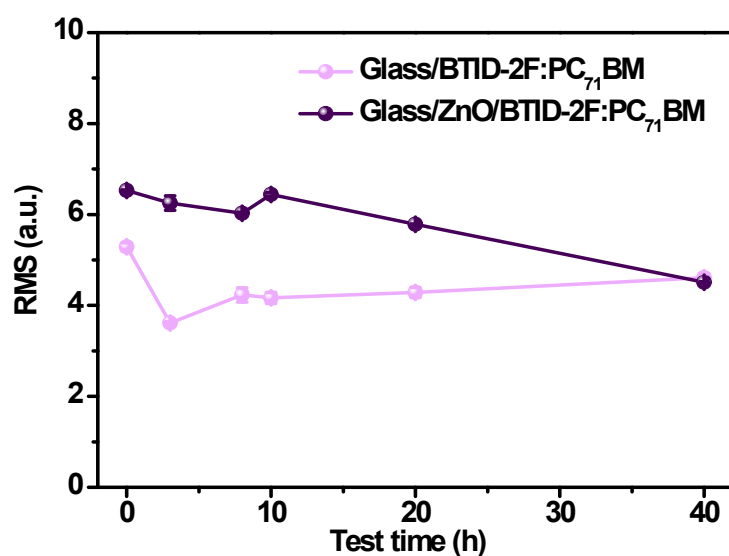
**Supplementary Figure 8.** The normalized  $V_{oc}$  of ITO/ZnO/BTID-2F:PC<sub>71</sub>BM/MoO<sub>3</sub>/Ag OSCs storage in ambient air measured under one sun illumination.



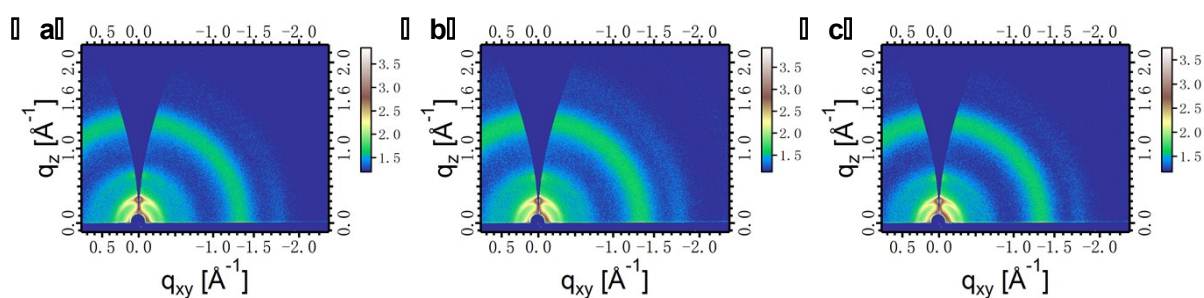
**Supplementary Figure 9.** The normalized  $V_{oc}$  of ITO/ZnO/BTID-2F:PC<sub>71</sub>BM/MoO<sub>3</sub>/Ag OSCs with different BHJ thickness during the storage time.



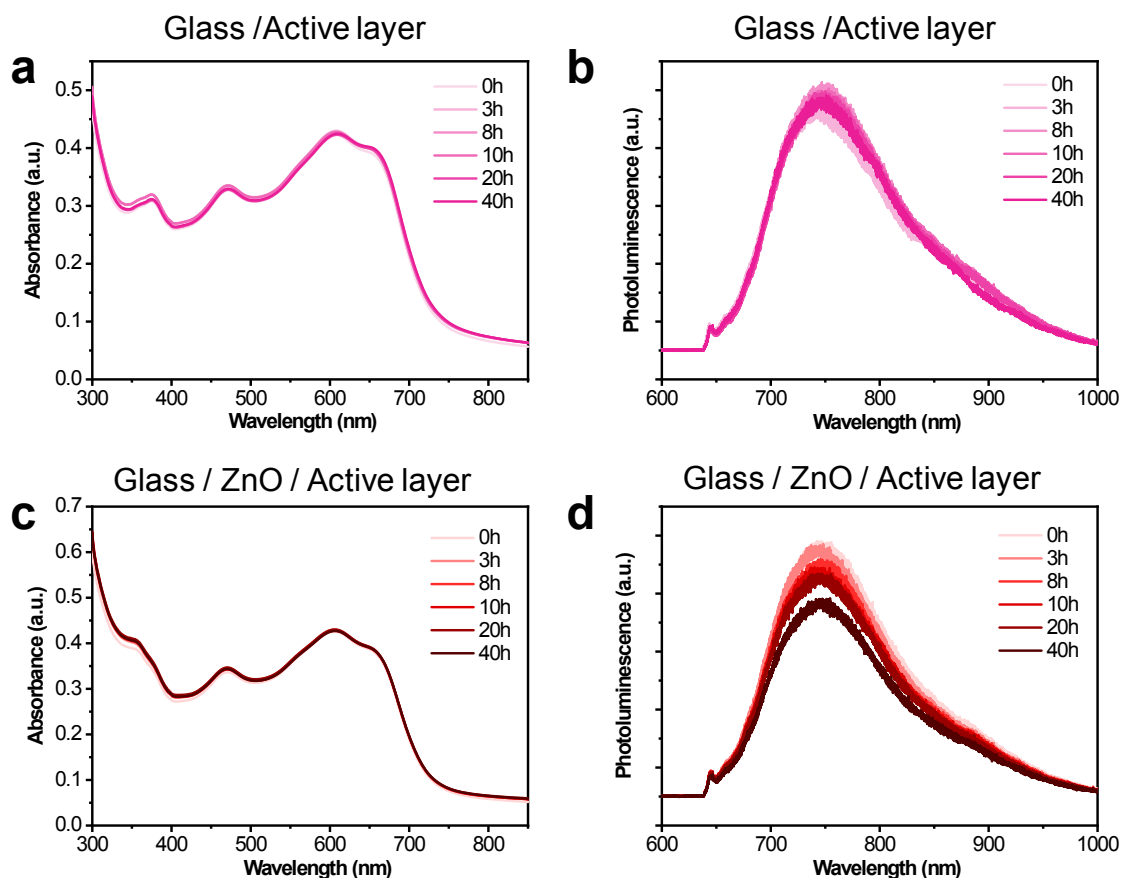
**Supplementary Figure 10.** AFM topography images of BTID-2F:PC<sub>71</sub>BM BHJ films measured under different time periods: Left, blends without ZnO layer; Right, blends with ZnO layer.



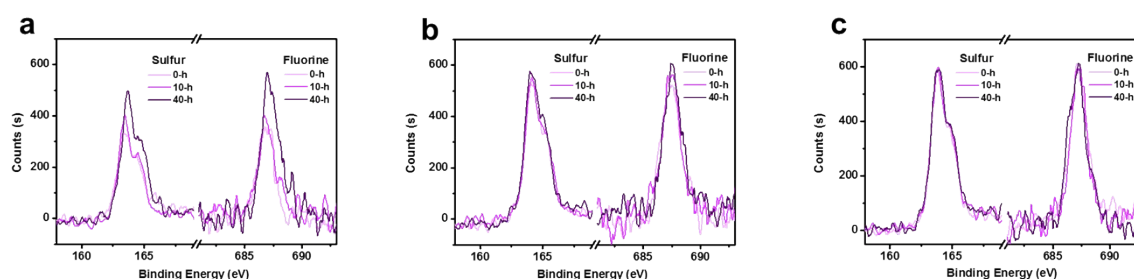
**Supplementary Figure 11.** The RMS for the glass/BHJ and glass/ZnO/BHJ films measured under different time periods.



**Supplementary Figure 12.** 2D GIWAXS patterns of the active layer coated on the top of ZnO layer with different time periods, including (a) 0h, (b) 24h, and (c) 48h, respectively.



**Supplementary Figure 13.** (a) The absorption spectra and (b) photoluminescence (PL) of active layer coated on the top of glass measured under different time periods; (c) The absorption spectra and (d) PL of active layer coated on the top of ZnO layer measured under different time periods. These samples were also stored in nitrogen glovebox.



**Supplementary Figure 14.** XPS spectra of BTID-2F:PC<sub>71</sub>BM layers with varying thickness (a) 8 nm (b) 17 nm and (c) 25 nm coated on the top of ZnO-modified Si wafer measured at different time periods, including 0h, 10h and 40h, respectively.

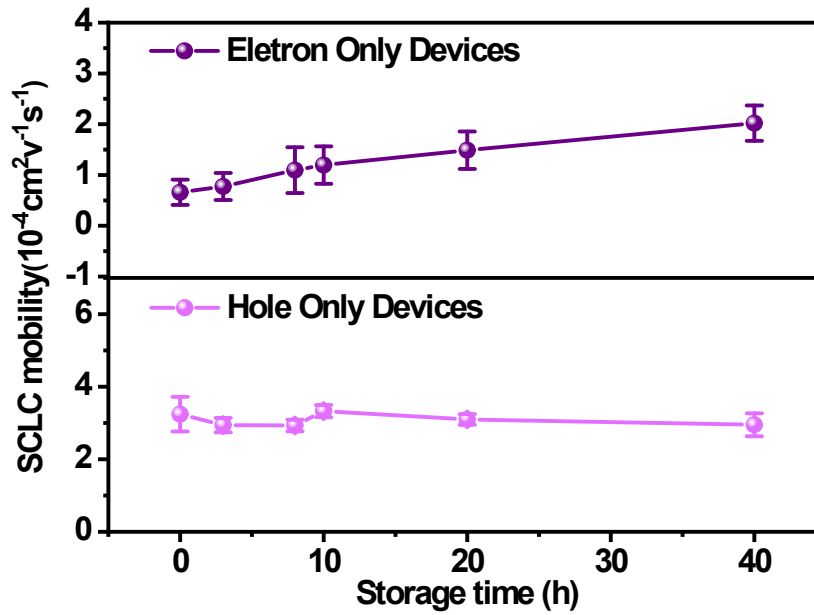
### Supplementary Note 1.

Charge carrier mobility is one of the major concerns in designing organic materials and in determining morphological changes in OSCs. High charge carrier mobility is preferred for

efficient transportation and photocurrent collection of the photoinduced charge carriers. We measured the hole only and electron only mobility of BTID-2F:PC<sub>71</sub>BM blend films in different time periods by the space-charge limited current (SCLC) method, to investigate the effect of interface changes on the hole and electron mobility. For the hole-only and electron-only devices, SCLC is described by:

$$J_{SCL} = \frac{9}{8} \epsilon_0 \epsilon_r \mu \frac{V_{in}^2}{L^3} \exp\left(-\frac{0.89 \times \beta}{\sqrt{L}} \sqrt{V}\right) \quad (1)$$

where  $J_{SCL}$  is the current density,  $\epsilon_0$  is the permittivity of free-space,  $\epsilon_r$  is the relative dielectric constant of the active layer,  $\mu$  is the charge carrier mobility,  $L$  is the thickness of the device and  $V_{in}$  is the voltage dropped across the sample.<sup>[14]</sup> The field dependent SCLC expression yielded a reasonably good fit to the measured  $J$ - $V$  curves of single-carrier devices. Supplementary Figure 15 presents the relevant hole-only and electron-only mobilities calculated from SCLC measurements on representative thin film devices at different time periods in a nitrogen atmosphere. The hole-only mobility is much stable, the electron-only mobility in contrast rises sharply during the same period. It demonstrated that a more suitable vertical phase separation at the BHJ/ZnO interface after long term storage could result in improved charge carrier properties.



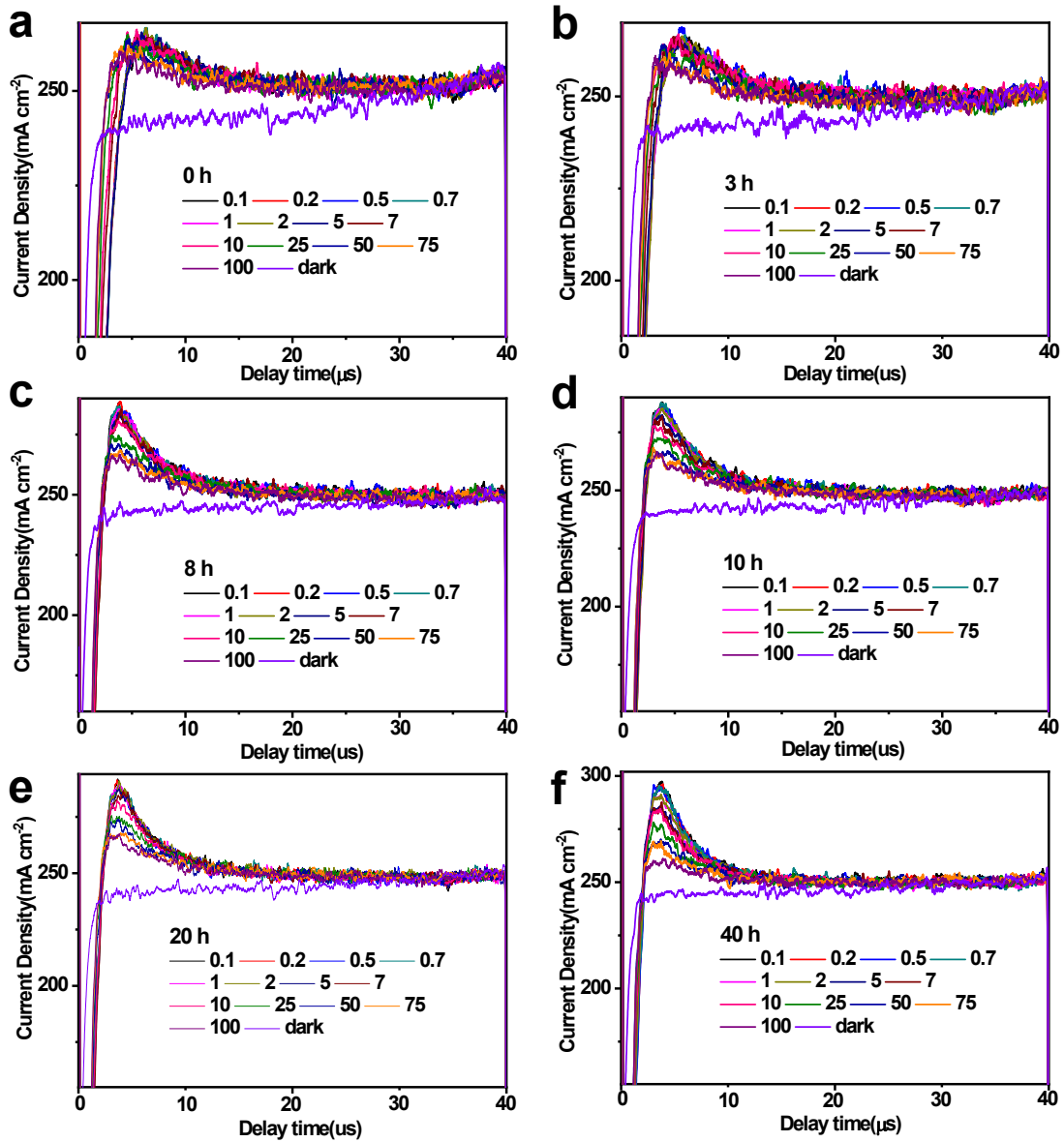
**Supplementary Figure 15.** Hole and electron only mobility as a function of storage time measured in single carrier diodes. Measurements were made on six devices of each type, and the error bars represent plus or minus 1 standard deviation from the mean.

### Supplementary Note 2.

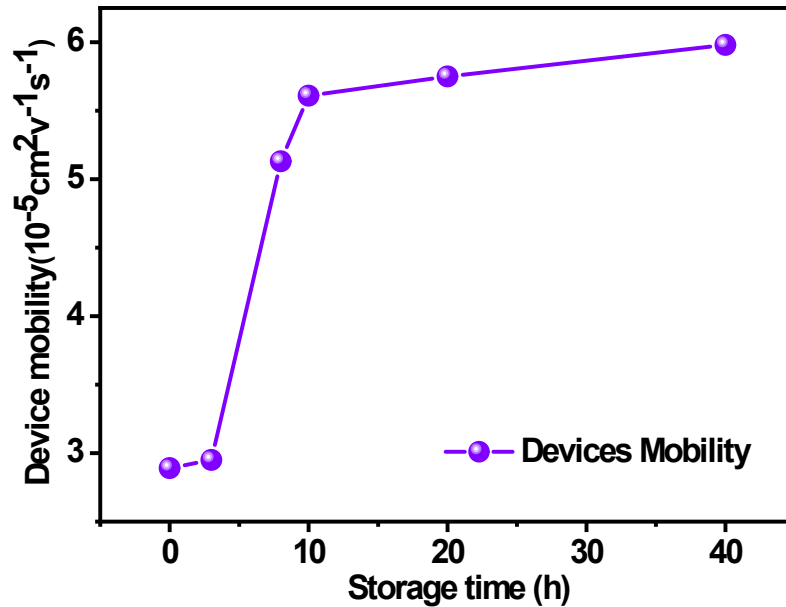
The photo-induced charge carrier extraction by linearly increasing voltage (photo-CELIV) technique is utilized to not only simultaneously determine the carrier lifetime and density, but also to gain a deeper understanding of the carrier transport and recombination loss dynamics.<sup>[15]</sup> When a reverse triangular-shaped bias is applied with an increasing rate  $A$  ( $\text{V s}^{-1}$ ) in the dark to low conductivity materials such as polymer solar cells, a rectangular-shaped current transient having a constant value is measured as an electrical signal. The constant current value of this transient stands for the capacitive displacement current  $j(0)$  ( $\text{C s}^{-1}$ ) of the sample. When the device is exposed to pulsed laser excitation, charge carriers are generated in the photoactive layer, and they either recombine or are extracted by the electric field. By measuring the maximum charge extraction current,  $t_{\text{max}}$ , which occurs at the maximum photocurrent and comparing the ratio of extracted current ( $\Delta j$ ) to constant current ( $j(0)$ ), we can calculate the charge carrier mobility using Equation 2:

$$\mu = \frac{2d^2}{3At_{max}^2[1 + 0.36\frac{\Delta j}{j(0)}]} \quad \text{if } \Delta j \leq j(0) \quad (2)$$

where  $d$  is the thickness of the active layer,  $A$  is the voltage rise speed  $A = dU/dt$ ,  $U$  is the applied voltage to the device. In this measurement, the applied maximum voltage is 2V, with active layer thickness around 110 nm, the maximum electric field is thus  $\sim 2 \times 10^5 \text{ Vcm}^{-1}$ . The Photo-CELIV transients recorded at room temperature at various delay times between the light pulse and the extraction pulse are shown in supplementary Figure 16. The average mobilities in devices are presented in supplementary Figure 17, and show a sustained improvement as storage time goes on.



**Supplementary Figure 16.** Photo-CELIV measurements on the (a) 0 h, (b) 3 h, (c) 8 h, (d) 10 h, (e) 20 h, and (f) 40 h stored devices for different delay times between the light pulse and the extraction voltage ramp.



**Supplementary Figure 17.** Carrier mobility of BTID-2F:PC<sub>71</sub>BM solar cells as a function of storage time calculated from photo-CELIV data.

**Supplementary Note 3.**

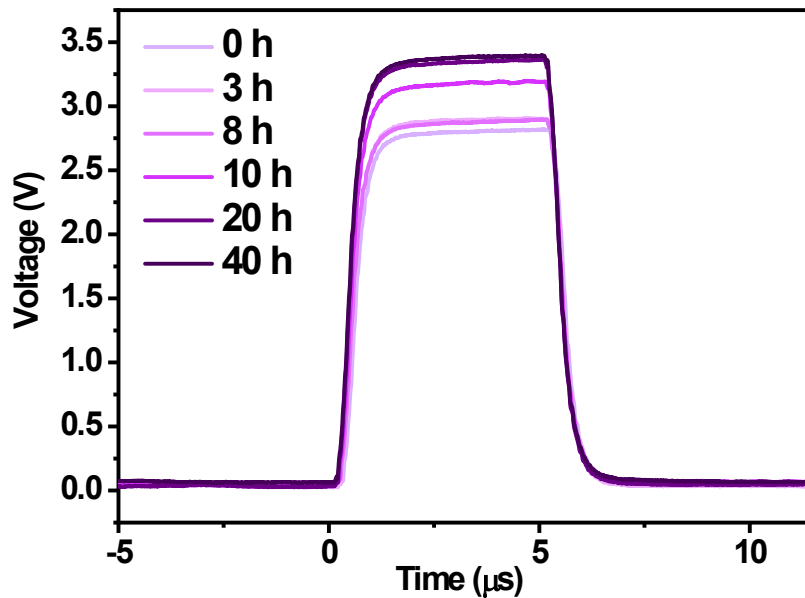
Transient photocurrent (TPC) measurement is a method for the time dependent extraction of photogenerated charge carriers. During the measurement the photocurrent decays very slowly due to the contribution of trapped charge carriers. In contrast to transient photovoltage, TPC measurements are conducted under short circuit condition and yield information about extractable charges, charge recombination and density of states. In addition, TPC measurements help to build “drift-diffusion” model which reflects trapping and detrapping of the photogenerated charges and the quality of contact between different layers. In the measurement, the sample device is in short circuit condition, the current is measured on a digital oscilloscope from the voltage across a small load resistor R and is valid for times longer than RC, where C is the sample capacitance.

TPC is an optoelectronic technique in which the device is held at short circuit under steady state conditions when a small short-lived perturbation is applied to the illumination level. Generally, the defined resistor is approximately 50 Ω to ensure that a measurable signal is produced ( $\Delta V >$

10 mV). Under laser illumination (here the wavelength of the laser is 405 nm), the photogenerated charges leave the device and create a TPC voltage transient that is measured through the 50  $\Omega$  resistor. This TPC transient is then converted into a current transient using Ohms law and integrated over the time to calculate the number of photogenerated charges ( $\Delta q$ ). This value of  $\Delta q$  can be correctly measured with TPC under the assumption of negligible charge carrier loss processes at short circuit. The total charge carrier density under open circuit conditions  $n(V_{oc})$  is calculated from

$$n(V_{oc}) = \frac{q(V_{oc})}{edA} \quad (3)$$

where  $A$  is the area of the device. Note that this analysis assumes that the charge density  $\Delta q$  generated by the laser excitation is the same at the short circuit and open circuit conditions and therefore is independent of device electric fields. As shown in Supplementary Figure 18, The photocurrent tail is a result of the slow recombination and de-trapping of trapped charges from a distribution of sub-gap energy states.<sup>[16]</sup>



**Supplementary Figure 18.** Measured transient photocurrents for the BTID-2F:PC<sub>71</sub>BM solar cells tested at different time periods. The illumination pulse intensity was 150 mW cm<sup>-2</sup> (a light pulse of 50  $\mu$ s).

#### Supplementary Note 4.

To further gain insight into the influence of spontaneous morphology evolution as a function of storage time on the device performance, we studied the light intensity dependence of current density-voltage ( $J$ - $V$ ) characteristics, which has been demonstrated to be a powerful tool for probing the dominant recombination mechanisms.<sup>[17]</sup> The  $J$ - $V$  characteristics of the solar cells under the illumination intensities ranging from 100 to 5 mW cm<sup>-2</sup> are tested.

In order to clear out the higher charge carrier density resulting from a reduction in the recombination rate, the light intensity dependence of  $J_{sc}$  and  $V_{oc}$  of BTID-2F:PC<sub>71</sub>BM solar cells under illumination intensities ranging from 100 to 5 mW cm<sup>-2</sup> are plotted in supplementary Figure 19a and 19b, respectively. A power law dependence of  $J_{sc}$  upon illumination intensity can be expressed as

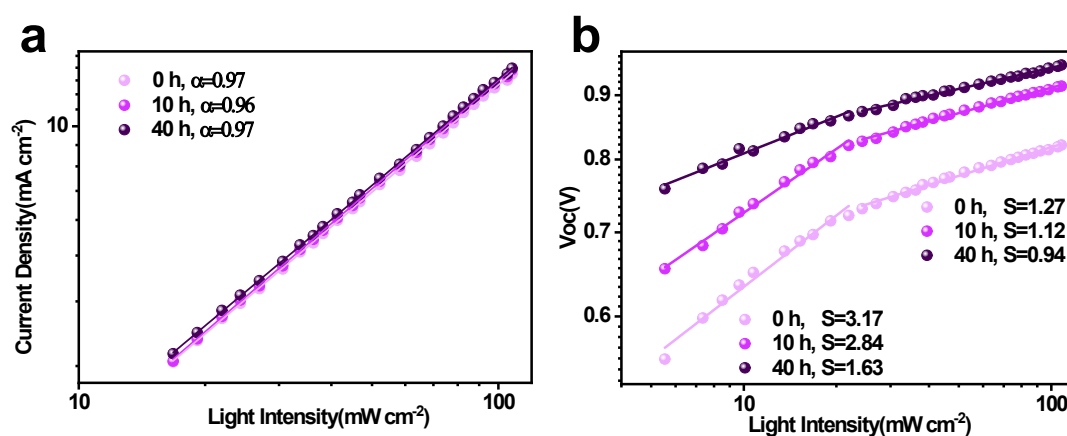
$$J_{sc} = \beta(I)^\alpha \quad (4)$$

Where  $\beta$  is a constant and  $\alpha$  is the exponential factor. The best fit for the data is obtained when the value  $\alpha$  is close to unity, which indicates negligible bimolecular recombination during sweep-out. As shown in supplementary Figure 19a, the fitting of the data based on the recombination kinetics at short circuit for three periods yield the slope ( $\alpha=0.97$ ) for the fresh device,  $\alpha=0.96$  for the device with 10 h stored period and  $\alpha=0.97$  for the device with 40 h stored period, indicating negligible changes of bimolecular recombination loss during sweep-out in the bulk.

Multiple studies have demonstrated that the light intensity dependence of the  $V_{oc}$  can directly provide insight into the role of trap-assisted recombination versus 2<sup>nd</sup> order recombination at the open circuit condition.<sup>[18]</sup> The  $V_{oc}$  and light intensity ( $I$ ) can be correlated by the following expression

$$V_{oc} = \frac{E_{gap}}{q} - \frac{kT}{q} \ln\left[\frac{(1-P)\gamma N_c^2}{PG}\right] \quad (5)$$

where  $E_{\text{gap}}$  is the energy difference between the HOMO of the electron donor and the LUMO of the electron acceptor,  $q$  is the elementary charge,  $k$  is the Boltzman constant,  $T$  is temperature in Kelvin,  $P$  is the dissociation probability of the electron-hole pairs into free carriers,  $\gamma$  the recombination constant,  $N_c$  the density of states in the conduction band, and  $G$  the generation rate of electron-hole pairs. This formula contains the dependence of the  $V_{\text{oc}}$  on the light intensity, as  $G$  is the only term directly proportional to the light intensity. Following the rules, the formula predicts a slope  $S = (kT/q)$  of the  $V_{\text{oc}}$  versus the natural logarithm of the incident light intensity. This implies that the slope of  $V_{\text{oc}}$  versus  $\ln(I)$  is equal to  $kT/q$  for 2<sup>nd</sup> order recombination. When trap-assisted recombination is involved, a stronger dependency of  $V_{\text{oc}}$  on the light intensity is observed and in this case, the slope of  $V_{\text{oc}}$  versus  $\ln(I)$  is equal to  $2 kT/q$ . Supplementary Figure 19b shows the  $V_{\text{oc}}$  versus light intensity relationship for devices as a function of stored time periods. For the fresh device, a strong dependence of  $V_{\text{oc}}$  on light intensity is observed where the recombination at the open circuit is a combination of monomolecular (slope =  $3.17 kT/q$ ) and bimolecular processes (slope =  $1.27 kT/q$ ). The Shockley-Read-Hall (SRH) recombination due to trap states can be clearly observed at low light intensities. The stored devices show the reduced trap assisted recombination with reduced slopes of  $1.12 kT/q$  and  $2.84 kT/q$  for 10 h device at high and low light intensities, respectively. A further reduced slopes at high and low light intensities can be found in the devices with 40 h stored time, implying that the density of traps at the BHJ/ZnO interface reduced effectively, and hence trap-assisted interface recombination is suppressed spontaneously.



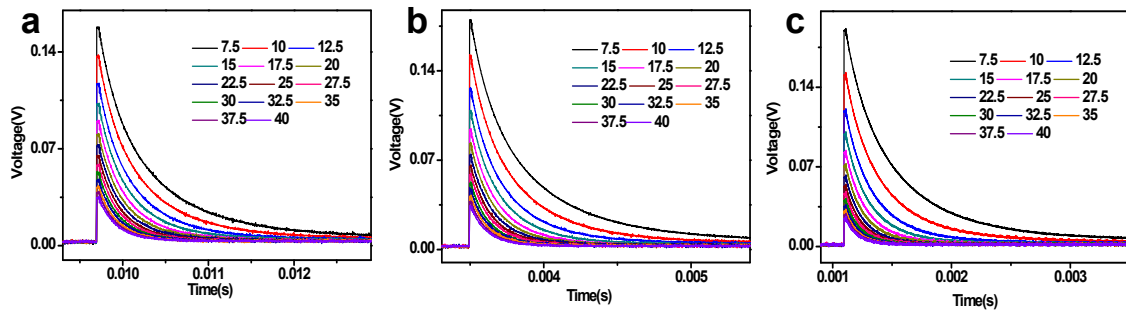
**Supplementary Figure 19.** The measured (a)  $J_{\text{sc}}$  and (b)  $V_{\text{oc}}$  of solar cells tested in different time periods, which plotted against illumination intensity on a logarithmic scale, together with linear fits to the  $J_{\text{sc}}$  and  $V_{\text{oc}}$  data (solid lines).

## Supplementary Note 5.

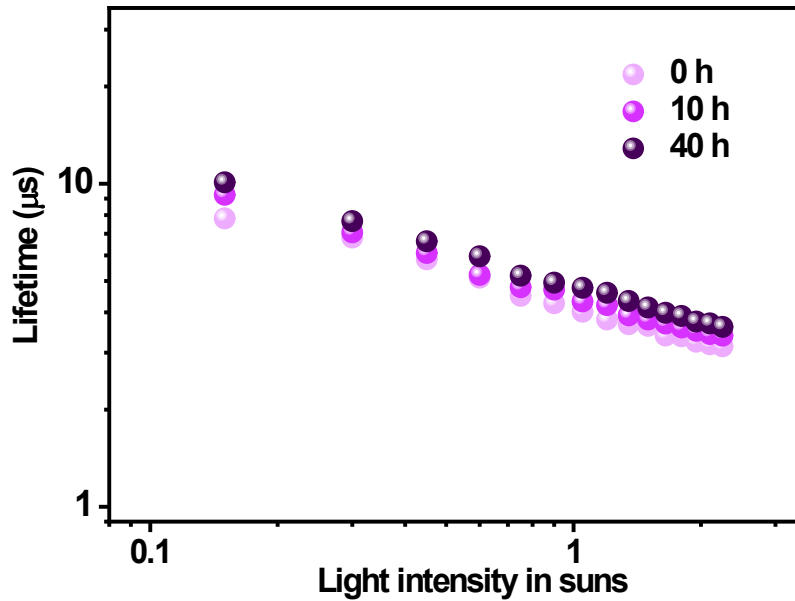
Transient photovoltage (TPV) is used to get information about charge carrier lifetime of a solar cell at different light intensities. The samples were connected to the terminal of an oscilloscope with the input impedance of 1 M $\Omega$  and continuously illuminated with a white light LED to control  $V_{oc}$ . The small perturbation is created by a 405nm diode laser, which is adjusted to keep the height of the photovoltage peak smaller than 15 mV resulting in a voltage transient with an amplitude  $\Delta V_0 \ll V_{oc}$ . Within the small perturbation regime, the transients exhibit single exponential decay, consistent with a pseudo-first-order rate equation of the form:<sup>[19]</sup>

$$\frac{d \Delta V}{dt} \propto \frac{d \Delta n}{dt} = -k_{eff} \Delta n = -\frac{\Delta n}{\tau_{\Delta n}} \quad (6)$$

Where  $\Delta V$  is the photovoltage,  $t$  is the time,  $\Delta n$  is the change in the density of photogenerated carriers density due to the perturbation pulse,  $k_{eff}$  is the pseudo-first order rate constant and  $\tau_{\Delta n}$  is the corresponding carrier lifetime. The  $\tau_{\Delta n}$  was determined from photovoltage transients recorded at different light bias from 0.15-2.5 suns. Supplementary Figure 20 exhibits the typical TPV measurements of a BTID-2F:PC<sub>71</sub>BM solar cell tested in different time periods, including 0h, 10h and 40h, respectively. Supplementary Figure 21 showed the TPV measurements of charge carrier lifetime in solar cells observed in different time periods.



**Supplementary Figure 20.** Transient photo-voltage measurements of a BTID-2F:PC<sub>71</sub>BM solar cell tested in different time periods, including (a) 0h, (b) 10h, and (c) 40h, respectively. The strong dependence of light intensity and lifetime can be observed.



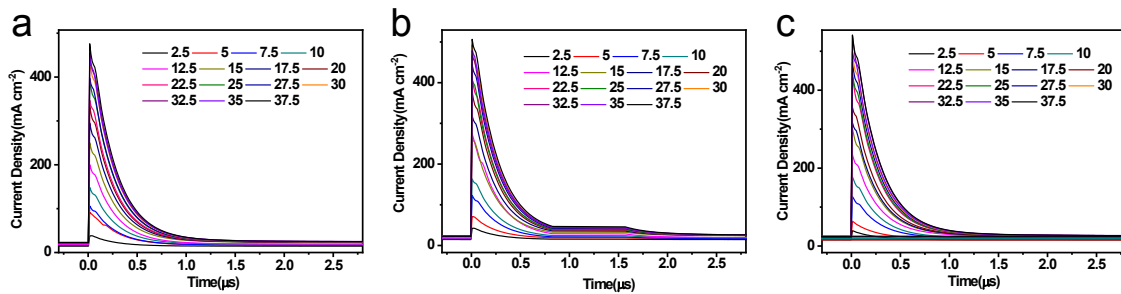
**Supplementary Figure 21.** Transient photo-voltage measurements of the charge carrier lifetime in a BTID-2F:PC<sub>71</sub>BM solar cell tested in different time periods, including 0h, 10h, and 40h, respectively.

### Supplementary Note 6.

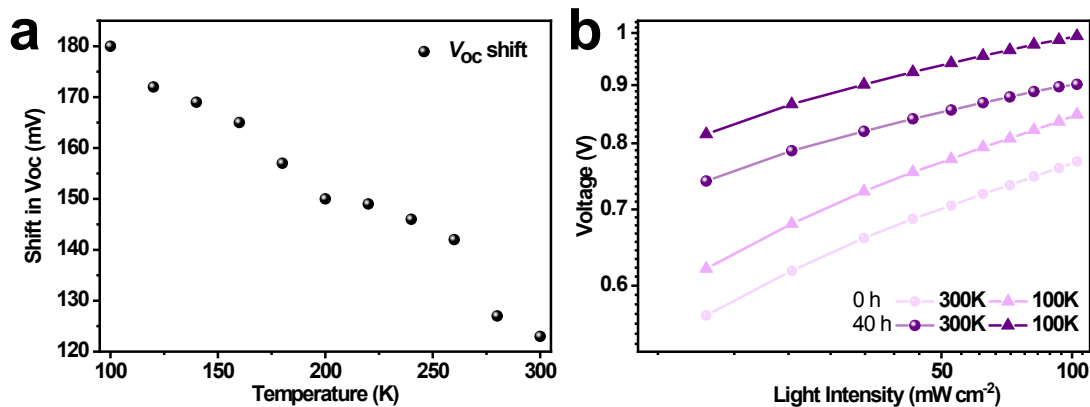
Charge extraction (CE) is a simple measurement technique to gain information about the stored charge in a device. CE allows us to quantify the amount of extractable charge present in the device at a given voltage, and thus provides information about the density of states. In the experiment, the solar cell is illuminated under open-circuit conditions, then the light is turned off and the cell is simultaneously switched to short-circuit conditions (<50 ns), extracting all mobile charge in the device. The current that is extracted from the device is integrated to calculate the charge carrier density that was present in the device before switching (seen in the Experimental Section). Most of the charge is extracted in a few microseconds due to a high internal electrical field at short circuit conditions. In order to get the charge density in the active layer,  $n_{active}$ , the total charge must be reduced by the so called geometrical charge density  $n_{geo}$ .

$$n_{active} = n_{ext.} - n_{geo.} = n_{ext.} - \frac{CV}{qdA} \quad (7)$$

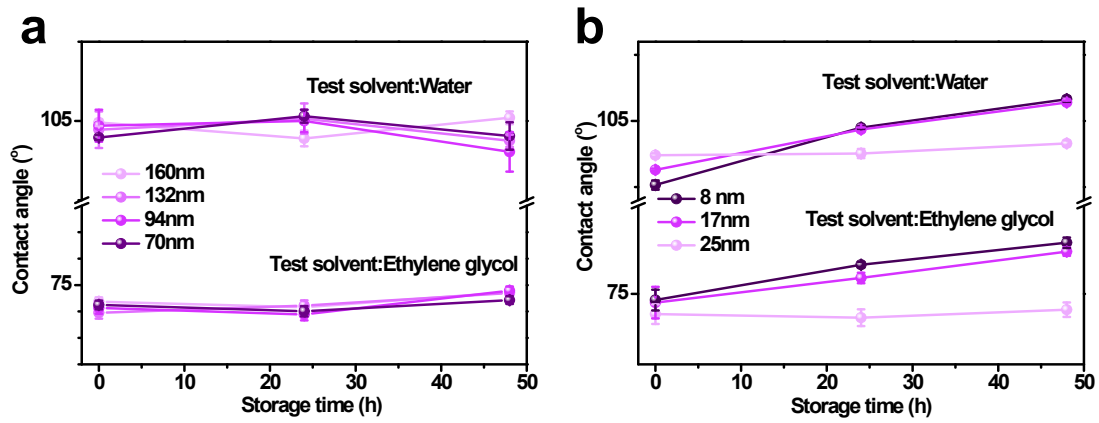
where  $n_{ext.}$  is the extracted charge density,  $C$  is the capacity,  $V$  is the applied voltage,  $q$  is the elementary charge,  $d$  is the thickness and  $A$  is the area of solar cell. Typical devices studied in this study with a thickness  $d=110$  nm, area  $A = 10.4$  mm<sup>2</sup>. Supplementary Figure 22 exhibits the typical CE measurements of a BTID-2F:PC<sub>71</sub>BM solar cell tested in different time periods, including 0h, 10h and 40h, respectively.



**Supplementary Figure 22.** Charge extraction measurements of a BTID-2F:PC<sub>71</sub>BM solar cell tested in different time periods, including (a) 0h, (b) 10h, and (c) 40h, respectively. The strong dependence of light intensity and carrier density can be observed.

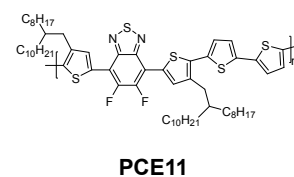
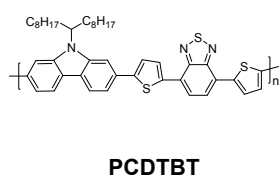
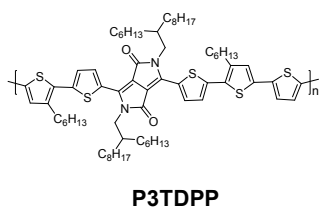
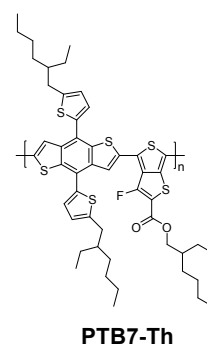
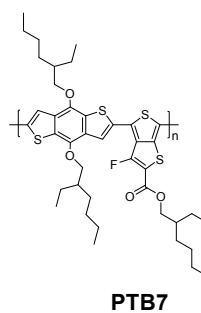
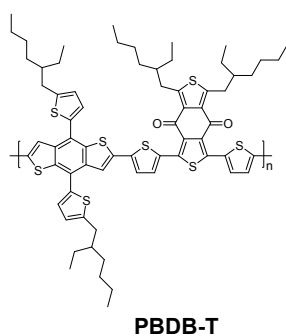
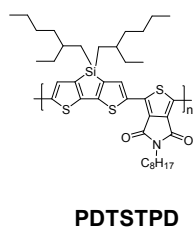
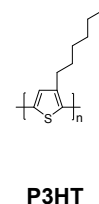
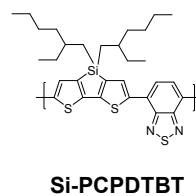
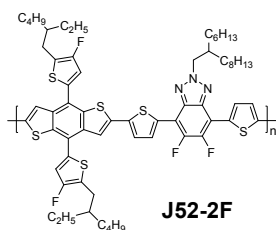
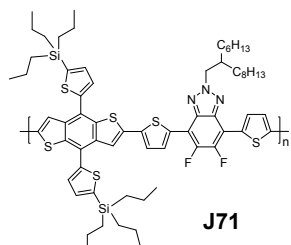
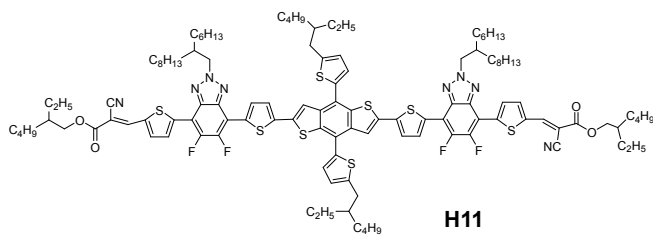
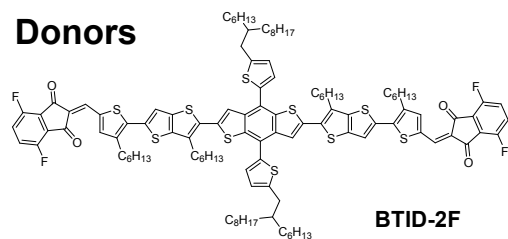


**Supplementary Figure 23.** (a) The shift in open-circuit voltage between fresh and stored solar cells. (b) The light intensity dependence of the fresh and stored curves is unchanged suggesting that there is no change in recombination mechanisms.

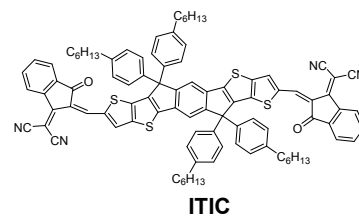
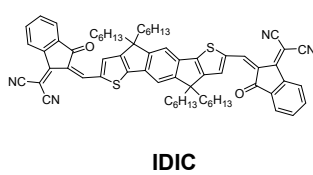
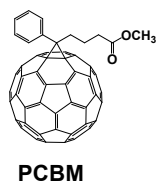


**Supplementary Figure 24.** The contact angle of ITO/ZnO/BTID-2F:PC<sub>71</sub>BM with (a) thicker films, (b) thinner films used two test solvent (water and ethylene glycol).

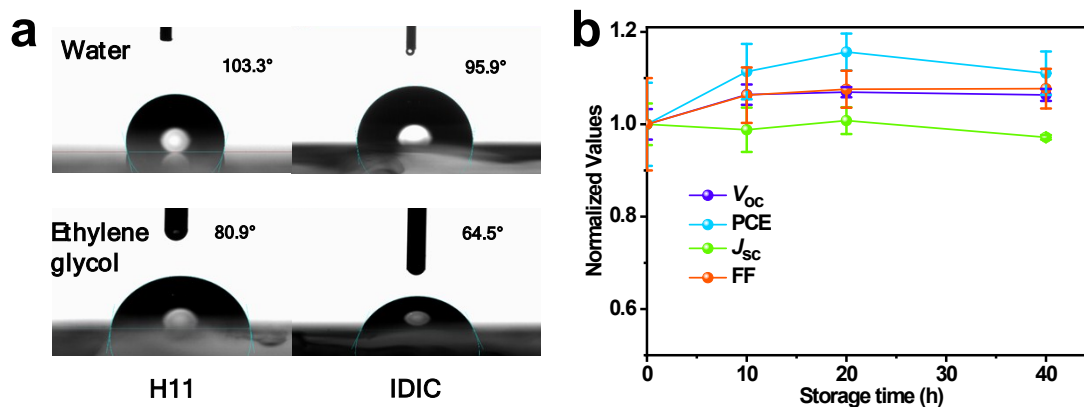
## Donors



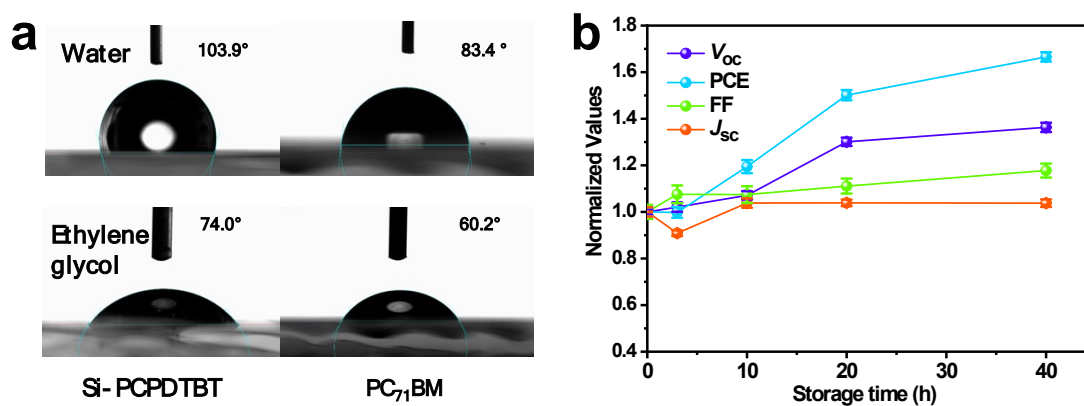
## Acceptors



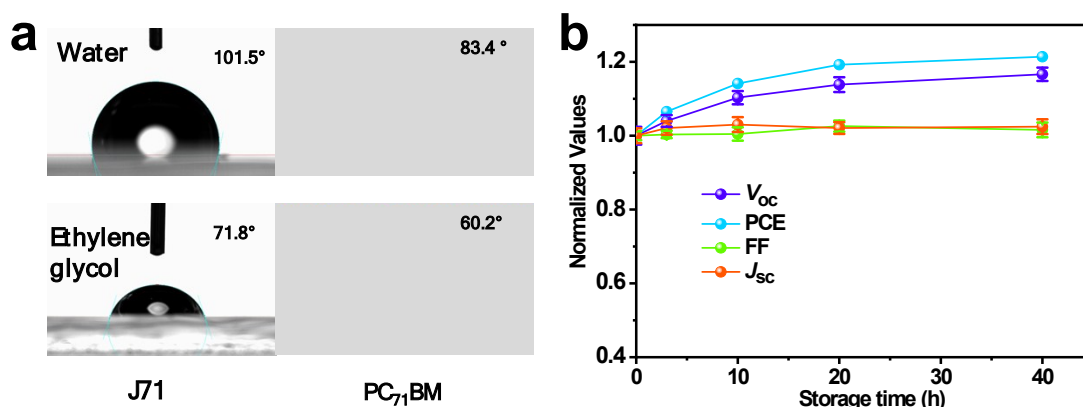
Supplementary Figure 25. Molecular structures of investigated donor and acceptor materials.



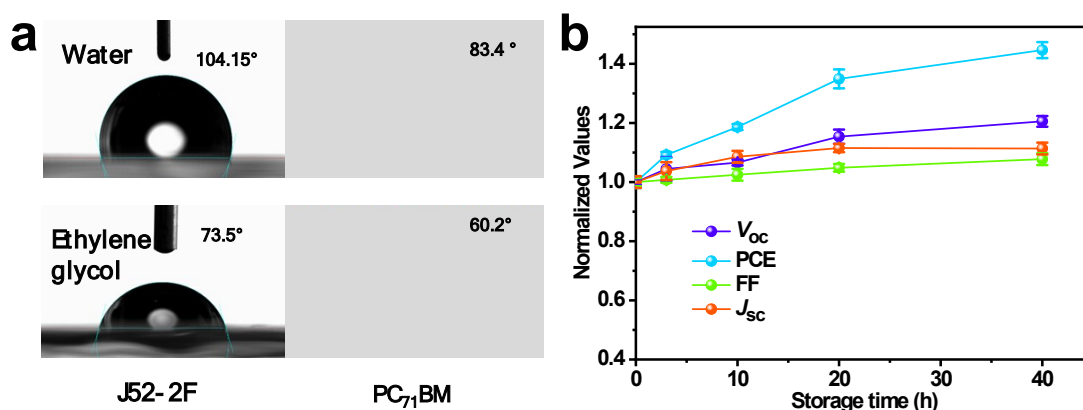
**Supplementary Figure 26.** (a) Photographs of water and ethylene glycol droplets on the top surfaces of H11 and IDIC films, and the respective contact angle values. (b) The normalized values of photovoltaic parameters of ITO/ZnO/H11:IDIC/MoO<sub>3</sub>/Ag OSCs over time measured under one sun illumination with different time periods. These samples were also stored in dark and in nitrogen glovebox.



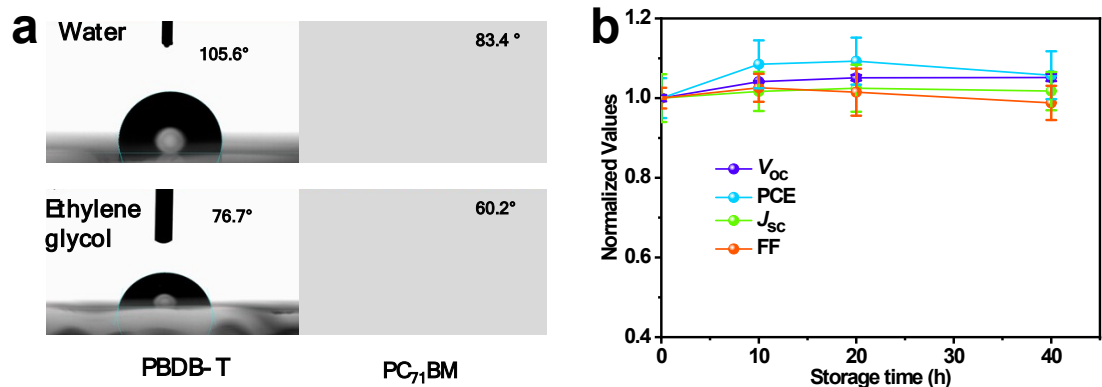
**Supplementary Figure 27.** (a) Photographs of water and ethylene glycol droplets on the top surfaces of Si-PCPDTBT and PC<sub>71</sub>BM films, and the respective contact angle values. (b) The normalized values of photovoltaic parameters of ITO/ZnO/Si-PCPDTBT:PC<sub>71</sub>BM /MoO<sub>3</sub>/Ag OSCs over time measured under one sun illumination with different time periods. These samples were also stored in dark and in nitrogen glovebox.



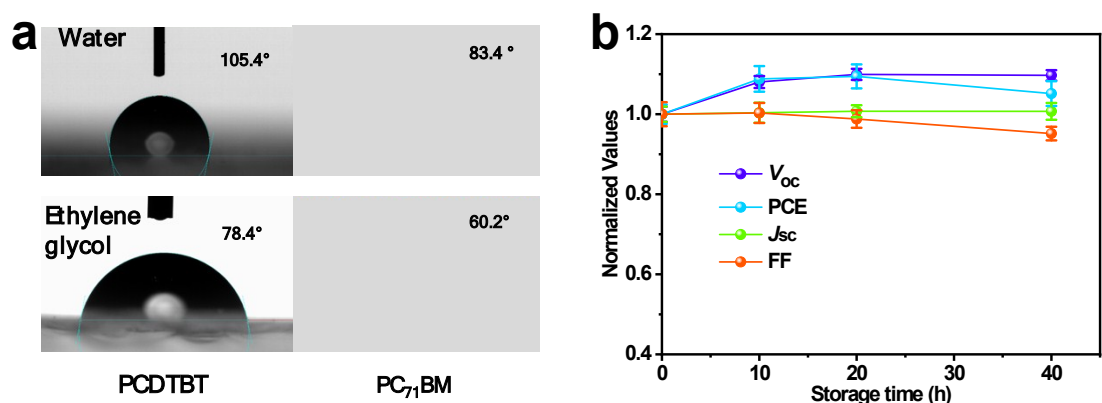
**Supplementary Figure 28.** (a) Photographs of water and ethylene glycol droplets on the top surfaces of J71 and PC<sub>71</sub>BM films, and the respective contact angle values. (b) The normalized values of photovoltaic parameters of ITO/ZnO/J71:PC<sub>71</sub>BM /MoO<sub>3</sub>/Ag OSCs over time measured under one sun illumination with different time periods. These samples were also stored in dark and in nitrogen glovebox.



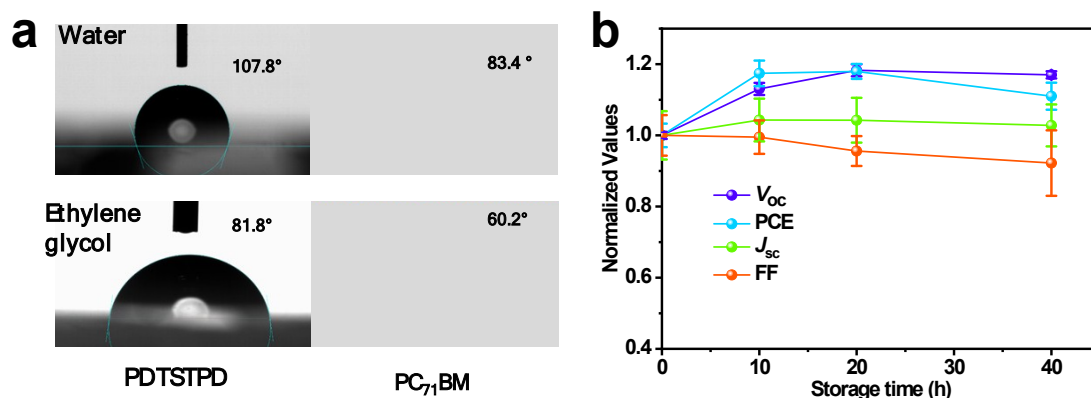
**Supplementary Figure 29.** (a) Photographs of water and ethylene glycol droplets on the top surfaces of J52-2F and PC<sub>71</sub>BM films, and the respective contact angle values. (b) The normalized values of photovoltaic parameters of ITO/ZnO/J52-2F:PC<sub>71</sub>BM /MoO<sub>3</sub>/Ag OSCs over time measured under one sun illumination with different time periods. These samples were also stored in dark and in nitrogen glovebox.



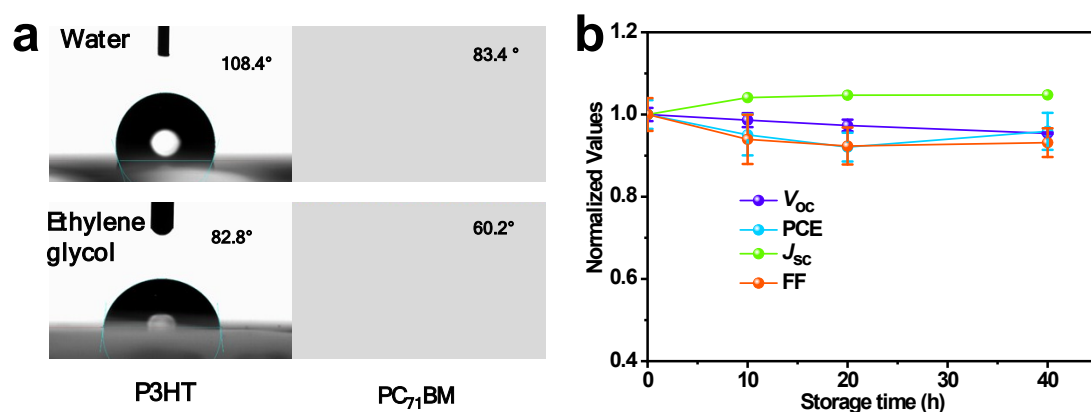
**Supplementary Figure 30.** (a) Photographs of water and ethylene glycol droplets on the top surfaces of PBDB-T and PC<sub>71</sub>BM films, and the respective contact angle values. (b) The normalized values of photovoltaic parameters of ITO/ZnO/PBDB-T:PC<sub>71</sub>BM /MoO<sub>3</sub>/Ag OSCs over time measured under one sun illumination with different time periods. These samples were also stored in dark and in nitrogen glovebox.



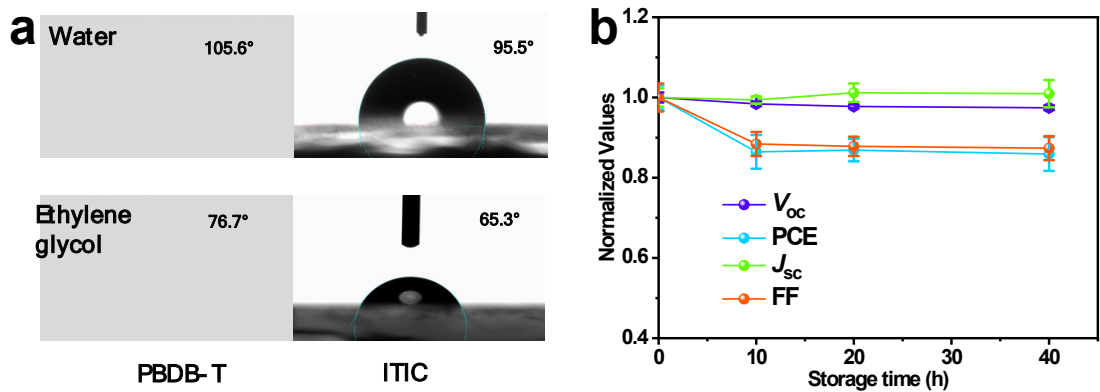
**Supplementary Figure 31.** (a) Photographs of water and ethylene glycol droplets on the top surfaces of PCDTBT and PC<sub>71</sub>BM films, and the respective contact angle values. (b) The normalized values of photovoltaic parameters of ITO/ZnO/PCDTBT:PC<sub>71</sub>BM /MoO<sub>3</sub>/Ag OSCs over time measured under one sun illumination with different time periods. These samples were also stored in dark and in nitrogen glovebox.



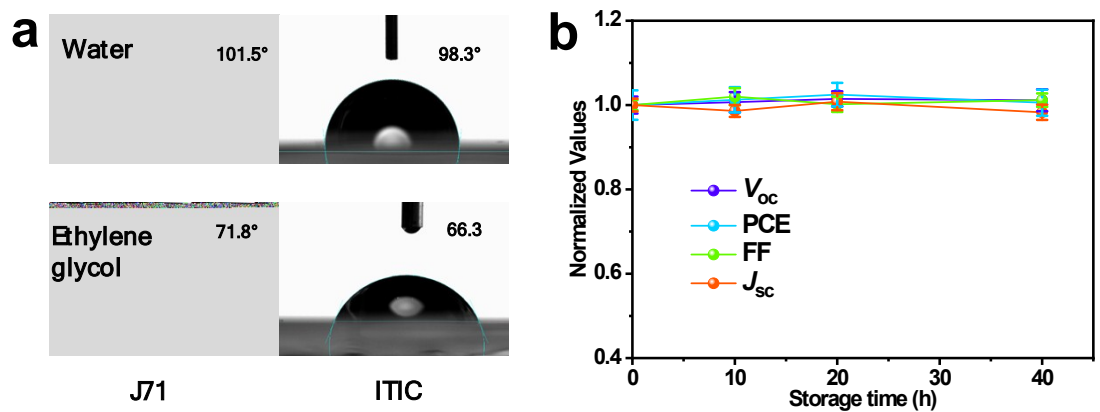
**Supplementary Figure 32.** (a) Photographs of water and ethylene glycol droplets on the top surfaces of PDTSTPD and PC<sub>71</sub>BM films, and the respective contact angle values. (b) The normalized values of photovoltaic parameters of ITO/ZnO/PDTSTPD:PC<sub>71</sub>BM /MoO<sub>3</sub>/Ag OSCs over time measured under one sun illumination with different time periods. These samples were also stored in dark and in nitrogen glovebox.



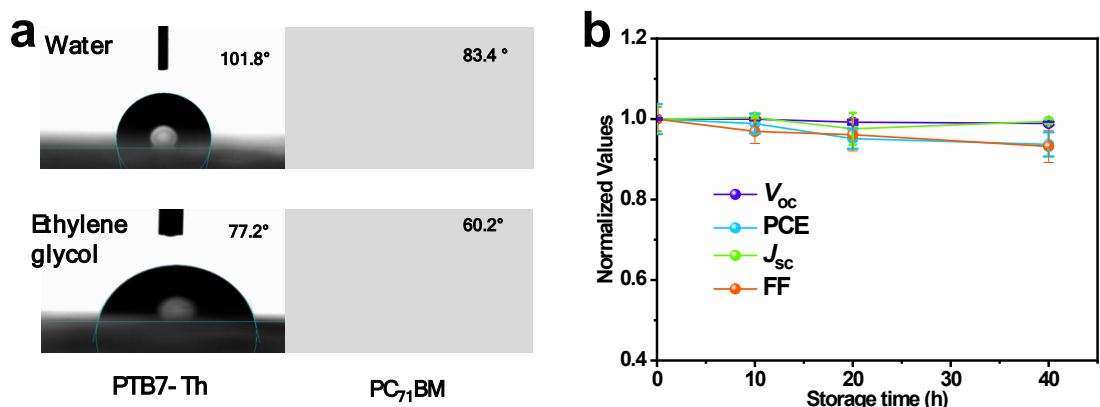
**Supplementary Figure 33.** (a) Photographs of water and ethylene glycol droplets on the top surfaces of P3HT and PC<sub>71</sub>BM films, and the respective contact angle values. (b) The normalized values of photovoltaic parameters of ITO/ZnO/P3HT:PC<sub>71</sub>BM/MoO<sub>3</sub>/Ag OSCs over time measured under one sun illumination with different time periods. These samples were also stored in dark and in nitrogen glovebox.



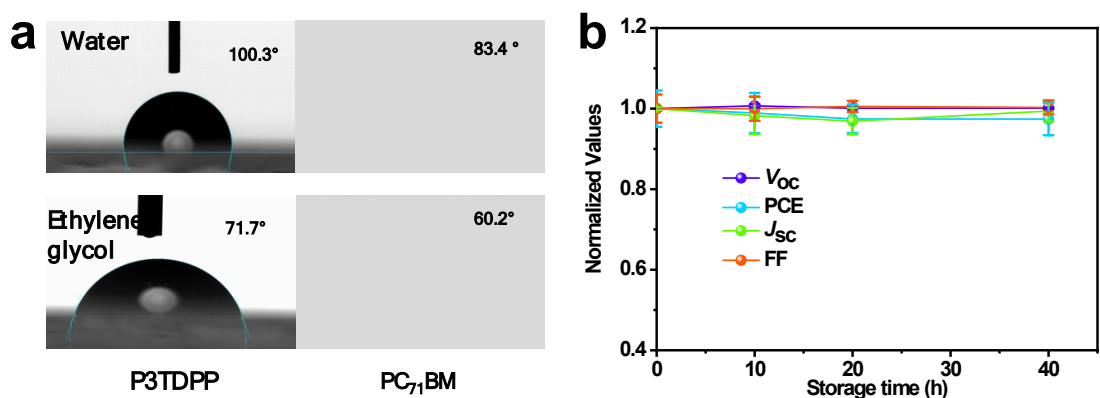
**Supplementary Figure 34.** (a) Photographs of water and ethylene glycol droplets on the top surfaces of PBDB-T and ITIC films, and the respective contact angle values. (b) The normalized values of photovoltaic parameters of ITO/ZnO/PBDB-T:ITIC/MoO<sub>3</sub>/Ag OSCs over time measured under one sun illumination with different time periods. These samples were also stored in dark and in nitrogen glovebox.



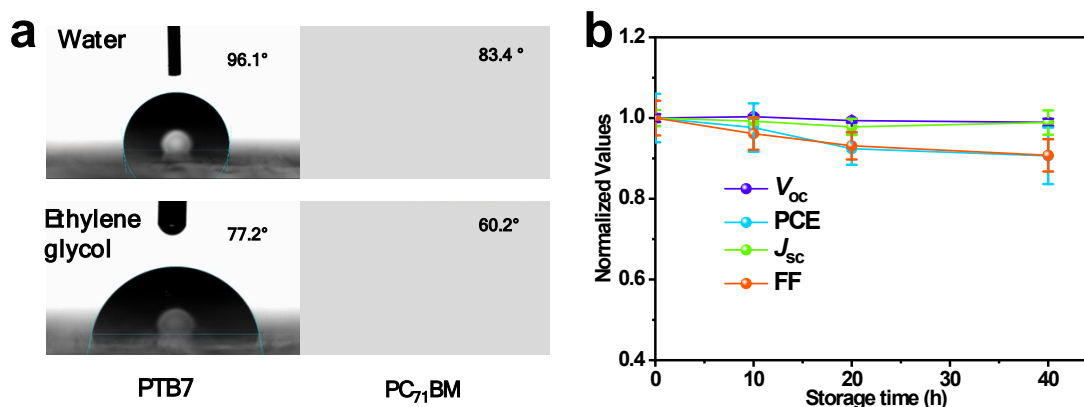
**Supplementary Figure 35.** (a) Photographs of water and ethylene glycol droplets on the top surfaces of J71 and ITIC films, and the respective contact angle values. (b) The normalized values of photovoltaic parameters of ITO/ZnO/J71:ITIC/MoO<sub>3</sub>/Ag OSCs over time measured under one sun illumination with different time periods. These samples were also stored in dark and in nitrogen glovebox.



**Supplementary Figure 36.** (a) Photographs of water and ethylene glycol droplets on the top surfaces of PTB7-Th and PC<sub>71</sub>BM films, and the respective contact angle values. (b) The normalized values of photovoltaic parameters of ITO/ZnO/PTB7-Th:PC<sub>71</sub>BM/Ag OSCs over time measured under one sun illumination with different time periods. These samples were also stored in dark and in nitrogen glovebox.



**Supplementary Figure 37.** (a) Photographs of water and ethylene glycol droplets on the top surfaces of PTB7-Th and PC<sub>71</sub>BM films, and the respective contact angle values. (b) The normalized values of photovoltaic parameters of ITO/ZnO/PTB7-Th:PC<sub>71</sub>BM/Ag OSCs over time measured under one sun illumination with different time periods. These samples were also stored in dark and in nitrogen glovebox.



**Supplementary Figure 38.** (a) Photographs of water and ethylene glycol droplets on the top surfaces of PTB7 and PC<sub>71</sub>BM films, and the respective contact angle values. (b) The normalized values of photovoltaic parameters of ITO/ZnO/PTB7:PC<sub>71</sub>BM/Ag OSCs over time measured under one sun illumination with different time periods. These samples were also stored in dark and in nitrogen glovebox.

**Supplementary Table 3.** The surface energies of materials estimated from the contact angles of ultrapure water and ethylene glycol on spin-coated films of materials.

Name	C.A. [°]		Surface energy [mJ/m <sup>2</sup> ]
	Water	Ethylene glycol	
<b>PEDOT:PSS</b>	16.4±1.3	16.7±0.9	122.77
<b>ZnO</b>	65.2±2.3	44.6±0.04	36.85
<b>BTID-2F</b>	103.5±1.1	75.3±0.08	43.17
<b>PC<sub>71</sub>BM</b>	83.4±0.4	60.2±1.2	29.22
<b>J71</b>	100.9±0.1	72.9±1.8	41.82
<b>J52-2F</b>	104.2±0.4	73.6±1.2	51.78
<b>Si-PCPDTBT</b>	103.9±0.2	56.0±1.1	135.79
<b>H11</b>	103.3±0	80.9±1.6	26.41
<b>P3HT</b>	108.4±0.7	82.8±0.1	35.50
<b>PBDB-T</b>	105.6±1.7	76.7±0.5	46.17
<b>IDIC</b>	95.9±0	64.5±0.1	50.93
<b>ITIC</b>	95.5±0.05	65.3±0.5	46.85
<b>PTB7</b>	96.1±0.1	77.2±0.3	20.47
<b>PTB7-Th</b>	101.8±0.2	77.2±0.2	32.22
<b>P3TDPP</b>	107.8±0.3	81.8±0	36.05
<b>PCDTBT</b>	100.3±0	71.7±0	43.58
<b>PDTSTPD</b>	105.4±0.1	78.4±0.1	39.95

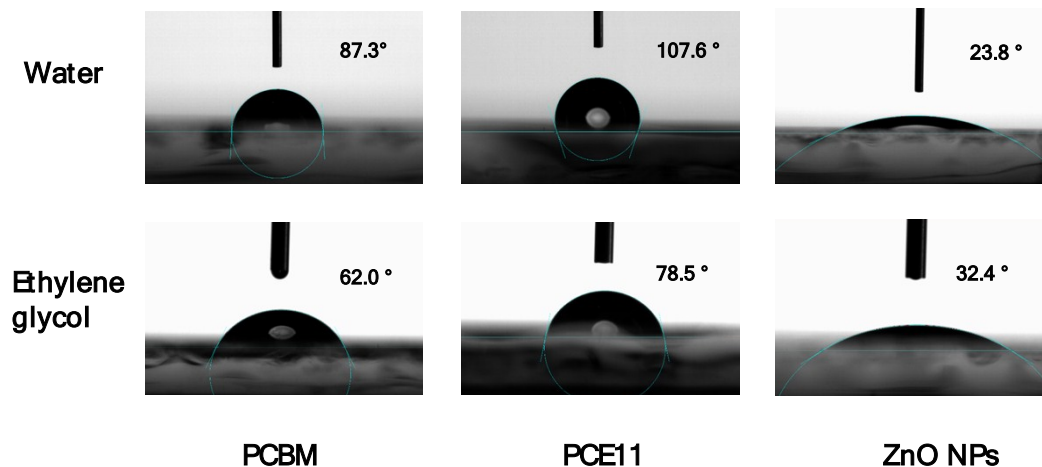
**Supplementary Table 4.** The Young's factors and wetting coefficients of PC<sub>71</sub>BM in BHJ/PDEOT:PSS interface in a conventional structure. For calculations, A refers to PEDOT:PSS, B refers to donor materials and C refers to acceptor materials.

Name	$\gamma_{C-B}$	$\gamma_{C-A}$	$\gamma_{A-B}$	$\omega_C$
------	----------------	----------------	----------------	------------

<b>BTID-2F:PC<sub>71</sub>BM</b>	20.33806	25.09752	0.249968	-19.04
----------------------------------	----------	----------	----------	--------

**Supplementary Table 5.** The Young's factors and wetting coefficients of fullerene and non-fullerene acceptors in relevant interfaces in inverted structures. For calculations, A refers to ZnO, B refers to donor materials and C refers to acceptor materials.

Active layers	No.	$\gamma_{C-B}$	$\gamma_{C-A}$	$\gamma_{A-B}$	$\omega_C$
<b>BTID-2F:PC<sub>71</sub>BM</b>	1	2.93	0.88	0.62	3.36
<b>H11:IDIC</b>	2	8.89	3.09	1.65	3.53
<b>Si-</b>	3	130.88	0.88	126.74	1.03
<b>PCPDTBT:PC<sub>71</sub>BM</b>					
<b>J71:PC<sub>71</sub>BM</b>	4	2.39	0.88	0.38	3.97
<b>J52-2F:PC<sub>71</sub>BM</b>	5	7.62	0.88	3.48	1.94
<b>PBDB-T:PC<sub>71</sub>BM</b>	6	4.31	0.88	1.34	2.55
<b>PCDTBT:PC<sub>71</sub>BM</b>	7	3.10	0.88	0.70	3.18
<b>PDTSTPD:PC<sub>71</sub>BM</b>	8	1.73	0.88	0.15	5.82
<b>P3HT:PC<sub>71</sub>BM</b>	9	0.59	0.88	0.028	-10.21
<b>PBDB-T:ITIC</b>	10	0.007	1.55	1.34	-1.15
<b>J71:ITIC</b>	11	0.14	1.55	0.38	-3.02
<b>PTB7-Th:PC<sub>71</sub>BM</b>	12	0.13	0.88	0.325	-2.28
<b>P3TDPP:PC<sub>71</sub>BM</b>	13	0.70	0.88	0.009	-17.52
<b>PTB7:PC<sub>71</sub>BM</b>	14	1.20	0.88	4.06	0.08



**Supplementary Figure 39.** Photographs of water and ethylene glycol droplets on the top surfaces of PCBM, PCE11 and ZnO nanoparticles films, and the respective contact angle values.

**Supplementary Table 6.** The surface energies of materials estimated from the contact angles of ultrapure water and ethylene glycol on spin-coated films of materials.

Name	C.A. [°]		Surface energy [mJ/m <sup>2</sup> ]
	Water	Ethylene glycol	
<b>PCBM</b>	87.3±0.2	62±0.1	32.38
<b>PCE11</b>	107.6±0.1	78.5±0.2	47.40

<b>ZnO NP</b>	23.8±0.2	32.4±0.2	135.97
---------------	----------	----------	--------

**Supplementary Table 7.** The Young's factors and wetting coefficients of PCBM in BHJ/ZnO NPs interface in a conventional structure. For calculations, A refers to PCBM, B refers to PCE11 and C refers to ZnO NPs.

Name	$\gamma_{C-B}$	$\gamma_{C-A}$	$\gamma_{A-B}$	$W_C$
<b>PCE11:PCBM</b>	1.43	35.64	22.81	-1.5

## REFERENCES

1. D. Deng, Y. Zhang, J. Zhang, Z. Wang, L. Zhu, J. Fang, B. Xia, Z. Wang, K. Lu, W. Ma and Z. Wei, *Nature communications*, 2016, 7, 13740.
2. H. Bin, Y. Yang, Z. G. Zhang, L. Ye, M. Ghasemi, S. Chen, Y. Zhang, C. Zhang, C. Sun, L. Xue, C. Yang, H. Ade and Y. Li, *Journal of the American Chemical Society*, 2017, 139, 5085-5094.
3. H. Bin, L. Gao, Z. G. Zhang, Y. Yang, Y. Zhang, C. Zhang, S. Chen, L. Xue, C. Yang, M. Xiao and Y. Li, *Nature communications*, 2016, 7, 13651.
4. Y. Cui, H. F. Yao, Y. C. Yang, Q. S. Zhang, H. J. Hou. *Acta Polymerica Sinica*, 2018, 2, 223-230.
5. J. Wang, F. Zhang, J. Xiao, F. Li, M. Zhang, Q. An and J. Zhang, *Journal of Materials Chemistry C*, 2016, 4, 7809-7816.
6. P. P. Khlyabich, B. Burkhart and B. C. Thompson, *Journal of the American Chemical Society*, 2011, 133, 14534-14537.
7. T. Y. Chu, J. Lu, S. Beaupre, Y. Zhang, J. R. Pouliot, S. Wakim, J. Zhou, M. Leclerc, Z. Li, J. Ding and Y. Tao, *Journal of the American Chemical Society*, 2011, 133, 4250-4253.
8. W. Zhao, D. Qian, S. Zhang, S. Li, O. Inganas, F. Gao and J. Hou, *Advanced materials*, 2016, 28, 4734-4739.
9. X. Ouyang, R. Peng, L. Ai, X. Zhang and Z. Ge, *Nature Photonics*, 2015, 9, 520-524.
10. Z. He, B. Xiao, F. Liu, H. Wu, Y. Yang, S. Xiao, C. Wang, T. P. Russell and Y. Cao, *Nature Photonics*, 2015, 9, 174-179.
11. F. Guo, N. Li, F. W. Fecher, N. Gasparini, C. O. Ramirez Quiroz, C. Bronnbauer, Y. Hou, V. V. Radmilovic, V. R. Radmilovic, E. Spiecker, K. Forberich and C. J. Brabec, *Nature communications*, 2015, 6, 7730.
12. J. S. Moon, J. Jo and A. J. Heeger, *Advanced Energy Materials*, 2012, 2, 304-308.
13. N. Li, J. D. Perea, T. Kassar, M. Richter, T. Heumueller, G. J. Matt, Y. Hou, N. S. Guldal, H. Chen, S. Chen, S. Langner, M. Berlinghof, T. Unruh and C. J. Brabec, *Nature communications*, 2017, 8, 14541.
14. J. Min, Y. N. Luponosov, N. Gasparini, M. Richter, A. V. Bakirov, M. A. Shcherbina, S. N. Chvalun, L. Grodd, S. Grigorian, T. Ameri, S. A. Ponomarenko and C. J. Brabec, *Advanced Energy Materials*, 2015, 5, 1500386.
15. T. M. Clarke, D. B. Rodovsky, A. A. Herzing, J. Peet, G. Dennler, D. DeLongchamp, C. Lungenschmied and A. J. Mozer, *Advanced Energy Materials*, 2011, 1, 1062-1067.
16. C. G. Shuttle, N. D. Treat, J. D. Douglas, J. M. J. Fréchet and M. L. Chabinyc, *Advanced Energy Materials*, 2012, 2, 111-119.

17. G. Zhang, R. Xia, Z. Chen, J. Xiao, X. Zhao, S. Liu, H.-L. Yip and Y. Cao, *Advanced Energy Materials*, 2018, 8, 1801609.
18. H. Cha, S. Wheeler, S. Holliday, S. D. Dimitrov, A. Wadsworth, H. H. Lee, D. Baran, I. McCulloch and J. R. Durrant, *Advanced Functional Materials*, 2018, 28, 1704389.
19. T. Heumueller, T. M. Burke, W. R. Mateker, I. T. Sachs-Quintana, K. Vandewal, C. J. Brabec and M. D. McGehee, *Advanced Energy Materials*, 2015, 5, 1500111.